e-ISSN 3050-9645
p-ISSN 2795-3274

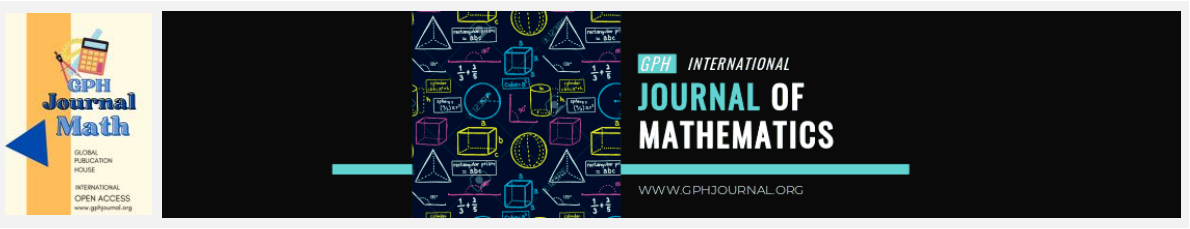

10.5281/zenodo.15630338 Vol. 8 Issue 03 March - 2025 Manuscript ID: #1945

Numerical Simulation and Fractional Order Analysis of COVID-19 Model with Treatment Intervention

I. G. Ezugorie

Department of Industrial Mathematics/Applied Statics,
Enugu State University of Science and Technology, Enugu, Nigeria

Abstract

COVID-19 remains a significant global health challenge, especially in regions where healthcare systems are strained and treatment accessibility varies. This study develops a fractional-order mathematical model for COVID-19 transmission that incorporates treatment effects to realistically capture disease control measures. Using Caputo fractional derivatives, the model effectively accounts for memory effects and complex time-dependent dynamics that classical integer-order models may overlook. The model's semi-analytical solution is obtained through the Adams–Bashforth–Moulton method, ensuring accurate and computationally efficient results. Analytical proofs confirm the existence, uniqueness, and boundedness of solutions, verifying the model's robustness. A thorough sensitivity analysis identifies critical parameters impacting COVID-19 spread, such as treatment rate and transmission coefficients. Simulation outcomes demonstrate that increasing treatment rate and reducing contact rate substantially decrease infection prevalence. Comparative studies reveal that the fractional-order model offers superior flexibility and precision over traditional integer-order models in representing COVID-19 dynamics. The Adams–Bashforth–Moulton method serves as an effective numerical technique for approximating model solutions, supporting its use in epidemic control strategies. The findings highlight the vital role of sustained treatment efforts combined with behavioural controls in mitigating COVID-19 transmission. This model provides a valuable framework for public health planning and can be adapted to other infectious diseases exhibiting memory-dependent transmission characteristics

Keywords and phrases:

COVID-19, Fractional-order modeling, Adams–Bashforth Moulton method, Sensitivity analysis, Numerical simulation.

How to cite: Ezugorie, I. G. (2025). Numerical Simulation and Fractional Order Analysis of COVID-19 Model with Treatment Intervention. *GPH-International Journal of Mathematics, 8*(03), 26-47. https://doi.org/10.5281/zenodo.15630338

Introduction

The outbreak of Coronavirus Disease 2019 (COVID-19), caused by the novel severe acute respiratory syndrome coronavirus 2 (SARS-CoV-2), emerged in Wuhan, China, in late 2019 and rapidly escalated into a global pandemic. The World Health Organization (WHO) declared COVID-19 a public health emergency of international concern in January 2020 and a global pandemic in March of the same year [1]. The virus spread rapidly across continents, overwhelming healthcare systems and disrupting social and economic activities worldwide. COVID-19 is primarily transmitted through respiratory droplets and aerosols during close person-to-person contact, though indirect transmission via contaminated surfaces has also been documented [2]. The disease presents a wide range of clinical symptoms, from asymptomatic and mild cases to severe respiratory distress and death, particularly among the elderly and those with underlying health conditions [3]. The emergence of new variants has further complicated transmission patterns and disease severity. To contain the spread of the virus, countries implemented a variety of public health interventions, including lockdowns, mask mandates, travel restrictions, and vaccination campaigns. Non-pharmaceutical interventions (NPIs) played a key role in the early phase of the pandemic, with studies indicating that strict NPIs could reduce transmission rates by up to 90% when effectively enforced [4]. The development and deployment of vaccines marked a major scientific milestone, though global disparities in vaccine access and hesitancy continue to pose challenges [5].

Mathematical modeling has been instrumental in analyzing the spread of COVID-19 and evaluating control strategies. Models such as the SEIR (Susceptible–Exposed–Infectious–Recovered) framework have been widely used to simulate epidemic dynamics and inform public health decisions. Recent models have integrated environmental and behavioral factors, improving predictive accuracy and supporting targeted interventions [6][7]. Despite significant progress in vaccine development and treatment strategies, COVID-19 remains a major global health concern. The continuous emergence of new variants, coupled with varying levels of immunity and healthcare infrastructure, underscores the need for sustained research, surveillance, and policy adaptation. Moving forward, combining vaccination, antiviral treatments, and dynamic public health responses will be essential in mitigating the long-term impact of the pandemic [8][9].

Fractional-order mathematical models leverage derivatives of non-integer order to capture memory and hereditary characteristics in dynamic systems—a notable enhancement over classic integer-order approaches. Such models are increasingly applied in fields like epidemiology, control systems, and viscoelastic materials, where past states significantly affect current dynamics [10]. The fractional framework allows for richer dynamical behaviors, such as long-term memory effects and anomalous diffusion, providing a more accurate description in many real-world systems compared to their integer-order counterparts [11]. A popular numerical technique for solving fractional differential equations is the Adams–Bashforth–Moulton method, a predictor–corrector scheme adapted specifically for fractional calculus [12]. This method combines the explicit Adams–Bashforth predictor with the implicit Adams–Moulton corrector to it eratively generate approximate solutions with relatively high accuracy and computational efficiency. Its effectiveness and stability have been demonstrated across various scientific applications, including modeling infectious disease dynamics, where it helps simulate fractional-order models that capture complex transmission patterns [13].

[14] developed a fractional-order SEIR model to study the dynamics of COVID-19 transmission incorporating quarantine and vaccination measures. They used Caputo fractional derivatives to capture memory effects in disease progression. The model's existence and

uniqueness of solutions were proven analytically. Numerical simulations were carried out using the Adams–Bashforth–Moulton method. The results showed that fractional-order models provided better fitting to real epidemic data compared to integer-order models, highlighting the impact of quarantine and vaccination rates in reducing disease spread. They concluded that fractional derivatives are effective in capturing complex dynamics and recommended fractional models for epidemic forecasting. **[15]** proposed a fractional-order SIRS model to analyze the effects of treatment and reinfection on tuberculosis transmission. They derived conditions for the stability of both disease-free and endemic equilibria using fractional Lyapunov techniques. Sensitivity analysis identified treatment rate and reinfection parameters as critical factors influencing disease prevalence. Their simulations demonstrated that increasing treatment rates led to a significant decrease in infectious individuals, while reinfection slowed disease elimination. They concluded that incorporating fractional calculus enhanced model realism and control strategy evaluation.[**16]** formulated a fractional-order SEIQR (Susceptible-Exposed-Infected-Quarantined-Recovered) model for dengue fever, incorporating vector dynamics and seasonal effects. The authors analyzed the model's stability using eigenvalue techniques and computed the basic reproduction number. Numerical solutions were obtained via the predictor-corrector method. Results indicated that fractional orders between 0.8 and 1 better captured seasonal fluctuations and disease persistence. The study concluded that fractional models are well-suited for diseases with environmental and temporal variability, and that quarantine measures effectively reduced infection peaks. [17] studied a fractional-order SI model for hepatitis B virus transmission, incorporating vaccination and treatment delays. They applied Laplace transform methods to prove solution existence and employed numerical simulations based on the Adams–Bashforth method. Their analysis revealed that fractional orders less than one significantly affected long-term disease dynamics. The model predicted that timely treatment combined with vaccination effectively lowered infection rates. The authors concluded that fractional-order models offer improved flexibility in describing disease latency and control interventions.

The main objective of this study was to develop and analyze a fractional-order mathematical model for COVID-19 transmission that incorporates treatment effects, aiming to capture the disease's complex, memory-dependent dynamics more accurately than classical models. The study sought to obtain a reliable semi-analytical solution using the Adams–Bashforth–Moulton method, investigate the model's mathematical properties, identify key parameters influencing disease spread through sensitivity analysis, and demonstrate the effectiveness of treatment and behavioral interventions in controlling the epidemic.

1.1 Preliminaries

This aspect explores fundamental ideas and results from the field of fractional calculus. In particular, we employ both left- and right-sided Caputo fractional derivatives, as detailed in references [18, 19, 20]. The study also emphasizes how fractional calculus can be effectively applied to model complex phenomena in diverse areas such as physics, engineering, biomathematics, and other branches of science

Definition 1: Let $f \in \Lambda^{\infty}(R)$, then the right and left Function's Caputo fractional derivative f is given by

$$ {}^{c}D_{t}^{\beta} f(t) = \left(t^{0}D_{t}^{-(a-\beta)} \left(\frac{d}{dt} \right)^{a} f(t) \right) $$

$$ {}^{a}D_{t}^{\beta} f(t) = \frac{1}{\Gamma(b-\beta)} \int_{0}^{t} \left((t-\lambda)^{b-\beta-1} f^{b}(\lambda) \right) d\lambda \tag{1} $$

In a similar vein

$$ {}_{T}^{a}D_{t}^{\beta} f(t) = \left({}_{t}^{a}D_{T}^{-(-\beta)} \left(\frac{-d}{dt} \right)^{a} f(t) \right) $$

$$ {}_{T}^{a}D_{T}^{\beta} f(t) = \frac{(-1)^{a}}{\Gamma(b-\beta)} \int_{t}^{T} \left((\lambda-t)^{b-\beta-1} f^{b}(\lambda) \right) d\lambda $$

Definition 2: The Mittag-Leffler function in generalized form $E_{\eta,\varepsilon}(x)$ for $x \in R$ is given by

$$ E_{\eta,\varepsilon}(x) = \sum_{b=0}^{\infty} \frac{x^{b}}{\Gamma(\eta b + \varepsilon)}, \phi, \varepsilon > 0 \tag{2} $$

This alternatively can be shown as

$$ E_{\eta,\varepsilon}(x) = xE_{\eta,\eta+\varepsilon(x)} + \frac{1}{\Gamma(\varepsilon)} \tag{3} $$

The function $t^{\varepsilon-1}E_{\eta,\varepsilon}(\pm\psi t^{\eta})$ is Laplace transformed as

$$ L\left[t^{\varepsilon-1}E_{\eta,\varepsilon(\pm\psi t^{\eta})} \right] = \frac{S^{\eta-\varepsilon}}{S^{\eta} \pm \psi} \tag{4} $$

Proposition 1.1. Let $f \in \Lambda^{\infty}(R) \cap d(R)$ and $\eta \in R,\ b-1 < \eta < b,$ Consequently, the following requirements are met:

1. $ {}_{t_0}^{a}D_{t}^{\beta} I^{\beta} f(t) = f(t) $
2. $ I_{t_0}^{\beta} D_{t}^{\beta} f(t) = f(t) - \sum_{k=0}^{b-k} \frac{t^{k}}{k!} f^{k}(t_o). $

1.1 Model formulation

This study presents a compartmental mathematical model designed to represent the transmission dynamics of COVID-19 within a population. The model divides the population into distinct compartments, each corresponding to a specific stage of the disease or group within the population. Using differential equations, it describes how individuals transition between these compartments over time, enabling the simulation of the epidemic's progression and the assessment of various intervention measures. The total population $N(t)$ is divided into six epidemiological compartment. The susceptible humans S(t) exposed humans E(t), the infected humans I(t), the deceased population D(t), individuals in treatment class T(t), recovered humans R(t). Suppose Λ denotes recruitment level that brings every individuals into the susceptible compartment. The susceptible population is decreased by λ where the exposed individuals progress to infectious class at the rate ε_1. ω and α_1 the treatment and disease induced death rate respectively and γ denotes recovery rate of infected individuals where α_2 represents burial rate of deceased humans and population of every compartment except $D(t)$ by the

natural death rate μ. Based on the model descriptions and figure 1. We have the following differential equations

$$\frac{dS}{dt} = \Lambda - (\lambda + \mu)S,$$
$$\frac{dE}{dt} = \lambda S - (\varepsilon_1 + \mu)E,$$
$$\frac{dI}{dt} = \varepsilon_1 E - (\alpha_1 + \omega + \mu)I,$$
$$\frac{dT}{dt} = \omega I - (\alpha_1 + \mu)T,$$
$$\frac{dD}{dt} = \alpha_1 I + \alpha_1 T - \alpha_2 D,$$
$$\frac{dR}{dtS} = \gamma T - \mu R. \qquad (5)$$

Where $\lambda = \frac{\phi(\mathrm{I}+\mathrm{D}+\mathrm{T})}{N}$

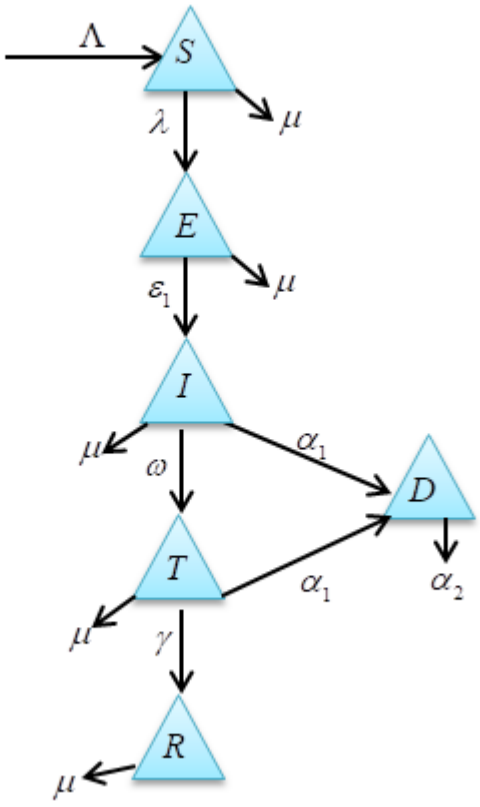

Figure1: schematic flow chart of the model

2.1 Fractional COVID-19 mathematical model

The integer-order COVID-19 model given in equation (5) by incorporating the Caputo fractional derivative operator. In contrast to the traditional model in equation (5), the fractional version provides increased adaptability, enabling a wider range of dynamic behaviors. The fractional modeling framework for COVID-19 is thus outlined as follows:

$$
\begin{aligned}
{}^{a}D_t^{\beta}S &= \Lambda-(\lambda+\mu)S,\\
{}^{a}D_t^{\beta}E &= \lambda S-K_1E,\\
{}^{a}D_t^{\beta}I &= \varepsilon_1E-K_2I,\\
{}^{a}D_t^{\beta}T &= \omega I-K_3T,\\
{}^{a}D_t^{\beta}D &= \alpha_1I+\alpha_1T-\alpha_2D,\\
{}^{a}D_t^{\beta}R &= \gamma T-\mu R.
\end{aligned}
$$

The force of infection for the covid-19 model is given as: $\lambda=\dfrac{\phi(\mathrm{I}+\mathrm{D}+\mathrm{T})}{N}$

Where; $K_1=(\varepsilon_1+\mu),\ K_2=(\alpha_1+\omega+\mu),\ K_3=(\alpha_1+\mu)$

Assuming favorable initial conditions

$$S(0)=S_0,E(0)=E_0,I(0)=I_0,T(0)=T_0,D(0)=D_0,R(0)=R_0. \quad (7)$$

3 Model Analysis

3.1. Positivity of model solution

Considering the non-negativity of the initial values.

$$\lim Sup.N(t)\le\frac{\Lambda}{\mu},$$

Suppose $\lim Sup.N_0(t)\le\dfrac{\Lambda}{\mu}$, then the feasible region of the model is given by:

$$\Omega=\left\{(S,E,I,T,D,R)\subset R_+^6: S+E+I+T+D+R\le\frac{\Lambda}{\mu}\right\}$$

$\Omega\subset R_+^6,$

Hence Ω is positively invariant.

If S_0,E_0,I_0,T_0,D_0,R_0 are non-negative. Therefore the solution of model (6) will also be non-negative for $t>0$. Taking the first equation from equation (6), we have that

$${}^{a}D_t^{\beta}S+(\lambda+\mu)S\ge\Lambda,$$

But $\Lambda\ge0,$ then

$${}^{a}D_t^{\beta}S+(\lambda+\mu)S\ge0,$$

Taking the Laplace transform;

$$L\left[{}^{a}D_t^{\beta}S\right]+L\left[(\lambda+\mu)S\right]\ge0$$

$$S^{\beta}S(s)-S^{\beta-1}S(0)+(\lambda+\mu)S(s)\ge0,$$

$$S(t) \geq \frac{S^{\beta-1}}{\left(S^{\beta}+(\lambda+\mu)\right)} S_0.$$

Taking the inverse Laplace transform yields

$$S(t) \geq E_{\beta,1}\left(-(\lambda+\mu)\right) S_0 \qquad (8)$$

Given that the term in equation (8) on the right is positive, we can now deduce that $S \geq 0$ for $t \geq 0$. Similarly, we have that $E \geq 0$, $I \geq 0, T \geq 0, D \geq 0, R \geq 0$ are positive. The solution will continue to be in R_{+}^{6} for all $t \geq 0$ with positive initial conditions.

3.2 Boundedness of solutions of the COVID-19 fractional –Order model.

The total population is given by:

$$N(t) = S(t) + E(t) + I(t) + T(t) + D(t) + R(t).$$

So that equation (6) gives

$$ {}^{a}D_t^{\beta} N(t) = {}^{a}D_t^{\beta} S(t) + {}^{a}D_t^{\beta} E(t) + {}^{a}D_t^{\beta} I(t) + {}^{a}D_t^{\beta} T(t) + {}^{a}D_t^{\beta} D(t) + {}^{a}D_t^{\beta} R(t).$$

$$ {}^{a}D_t^{\beta} N(t) = \Lambda - \mu N(t) \qquad (9)$$

Taking Laplace transformation equation (9) yields

$$L\left[{}^{a}D_t^{\beta} N(t)\right] \leq L\left[\Lambda - \mu N(t)\right],$$

$$S^{\beta} N(S) - S^{\beta-1} N(0) + \mu N(S) \leq \tfrac{\Lambda}{S},$$

$$N(\mathrm{s}) \leq \frac{S^{\beta-1}}{\left(S^{\beta}+\mu\right)} N(0) + \frac{\Lambda}{S\left(S^{\beta}+\mu\right)} \qquad (10)$$

Taking inverse Laplace transform of equation (10) gives

$$N(t) \leq E_{\beta,1}\left(-\mu t^{\beta}\right) N(0) + \Lambda E_{\beta,\beta+1}\left(-\mu t^{\beta}\right)$$

At $t \to \infty$, the limit of equation (11) yields

$$\lim_{t\to\infty} Sup N(t) = \frac{\Lambda}{\mu}.$$

This means that, if $N \leq \frac{\Lambda}{\mu}$ then $N(t) \leq \frac{\Lambda}{\mu}$ which implies that, $N(t)$ is bounded.

3.3 Existence and uniqueness of solutions of the model

Let T be a real nonnegative number, given that X = [0, T]. The collection of every continuous function defined on X is denoted by $N_e^0 X$ with norm as

$$\|J\| = \sup\left\{\left|J(t)\right| t, \in X\right\}.$$

Taking into account model (6) with the initial conditions in (7) gives

$$ {}^{a}D_t^{\beta} J(t) = J\left(t, G(x)\right), 0 < t < T < \infty,$$

$$J(0) = J_0. \qquad (12)$$

Where $J(t)=\left(S(t),E(t),I(t),T(t),D(t),R(t)\right)$ denotes the classes, and G is a continuous function with the following definition;

$$B_1\left(t,B(t)\right)=\begin{pmatrix}B_1\left(t,S(t)\right)\\B_2\left(t,E(t)\right)\\B_3\left(t,I(t)\right)\\B_4\left(t,T(t)\right)\\B_5\left(t,D(t)\right)\\B_6\left(t,B(t)\right)\end{pmatrix}=\begin{pmatrix}\Lambda-\left(\frac{\phi(\mathrm{I}+\mathrm{D}+\mathrm{T})}{N}\right)S+\mu S\\\left(\frac{\phi(\mathrm{I}+\mathrm{D}+\mathrm{T})}{N}\right)S-(\varepsilon_1+\mu)E\\\varepsilon_1E-(\alpha_1+\omega+\mu)I\\\omega I-(\alpha_1+\mu)T\\\alpha_1I+\alpha_1T-\alpha_2D\\\gamma T-\mu R\end{pmatrix} \tag{13}$$

Using proposition (2.1), yields,

$$\begin{aligned}S(t)&=S_0+I_t^{\beta}\left[\Lambda-\left(\frac{\phi(\mathrm{I}+\mathrm{D}+\mathrm{T})}{N}\right)S+\mu S\right],\\E(t)&=E_0+I_t^{\beta}\left[\left(\frac{\phi(\mathrm{I}+\mathrm{D}+\mathrm{T})}{N}\right)S-(\varepsilon_1+\mu)E\right],\\I(t)&=I_0+I_t^{\beta}\left[\varepsilon_1E-(\alpha_1+\omega+\mu)I\right],\\T(t)&=T_0+I_t^{\beta}\left[\omega I-(\alpha_1+\mu)T\right],\\D(t)&=D_0+I_t^{\beta}\left[\alpha_1I+\alpha_1T-\alpha_2D\right],\\R(t)&=R_0+I_t^{\beta}\left[\gamma T-\mu R\right].\end{aligned} \tag{14}$$

The Picard iteration of (14) is given below

$$\begin{aligned}S(t)&=S_0+\frac{1}{\Gamma(\beta)}\int_0^t(t-\lambda)^{\beta-1}B_1\left(\lambda,S_{n-1}(\lambda)\right)d\lambda,\\E(t)&=E_0+\frac{1}{\Gamma(\beta)}\int_0^t(t-\lambda)^{\beta-1}B_2\left(\lambda,E_{n-1}(\lambda)\right)d\lambda,\\I(t)&=I_0+\frac{1}{\Gamma(\beta)}\int_0^t(t-\lambda)^{\beta-1}B_3\left(\lambda,I_{n-1}(\lambda)\right)d\lambda,\\T(t)&=T_0+\frac{1}{\Gamma(\beta)}\int_0^t(t-\lambda)^{\beta-1}B_4\left(\lambda,T_{n-1}(\lambda)\right)d\lambda,\\D(t)&=D_0+\frac{1}{\Gamma(\beta)}\int_0^t(t-\lambda)^{\beta-1}B_5\left(\lambda,D_{n-1}(\lambda)\right)d\lambda,\\R(t)&=R_0+\frac{1}{\Gamma(\beta)}\int_0^t(t-\lambda)^{\beta-1}B_6\left(\lambda,R_{n-1}(\lambda)\right)d\lambda.\end{aligned} \tag{15}$$

Changing the initial value problem in equation (12) yields ;

$$J(t)=J(0)+\frac{1}{\Gamma(\beta)}\int_0^t(t-\lambda)^{\beta-1}B\left(\lambda,B(\lambda)\right)d\lambda. \tag{16}$$

Lemma 1. The vector $B\left(t,J\left(t\right)\right)$ satisfies the Lipchitz r on a set $\left[0,T\right]\times R_{+}^{6}$ with the Lipschitz constant given as;

$$\Im=\max\left(\left(I^{*}+D^{*}+T^{*}+\mu\right),(\varepsilon_{1}+\mu),(\alpha_{1}+\omega+\mu),(\alpha_{1}+\mu)\right)$$

Proof

$$\left\|B_{1}\left(t,S\right)-B_{1}\left(t,S\right)\right\|$$

$$\left\|\Lambda-\left(\frac{\phi(I+D+T)}{N}\right)S+\mu S\right\|$$

$$\left\|-\left(\Lambda-\left(\frac{\phi(I+D+T)}{N}\right)+\mu\right)S\right\|$$

$$\left\|-\left(\frac{\phi(I+D+T)}{N}\right)\left(S-S_{1}\right)+\mu\left(S-S_{1}\right)\right\|$$

$$\leq\left(\phi^{*}\right)\left\|\left(S-S_{1}\right)\right\|+\left\|\mu\left(S-S_{1}\right)\right\|$$

$$\therefore\left\|B_{1}\left(t,S\right)-B_{1}\left(t,S_{1}\right)\right\|\leq\left(\phi^{*}+\mu\right)\left\|S-S_{1}\right\|.$$

So that:

$$\left\|B_{2}\left(t,E\right)-B_{2}\left(t,E_{1}\right)\right\|\leq(\varepsilon_{1}+\mu)\left\|E-E_{1}\right\|,$$

$$\left\|B_{3}\left(t,I\right)-B_{3}\left(t,I_{1}\right)\right\|\leq(\alpha_{1}+\omega+\mu)\left\|I-I_{1}\right\|,$$

$$\left\|B_{4}\left(t,T\right)-B_{4}\left(t,T_{1}\right)\right\|\leq(\alpha_{1}+\mu)\left\|T-T_{1}\right\|,$$

$$\left\|B_{5}\left(t,D\right)-B_{5}\left(t,D_{1}\right)\right\|\leq\alpha_{2}\left\|D-D_{1}\right\|,$$

$$\left\|B_{6}\left(t,R\right)-B_{6}\left(t,R_{1}\right)\right\|\leq\mu\left\|R-R_{1}\right\|.$$

And

$$\left\|B\left(t,J\left(t\right)\right)-B\left(t,J_{2}\left(t\right)\right)\right\|\leq\Im\left\|J_{1}-J_{2}\right\|.$$

$$\Im=\max\left(\left(I^{*}+D^{*}+T^{*}+\mu\right),(\varepsilon_{1}+\mu),(\alpha_{1}+\omega+\mu),(\alpha_{1}+\mu)\right)\quad(18)$$

Lemma 2: There is a solution to the initially value problems (6), (7) in equation (18).

$J\left(t\right)\in L_{c}^{0}\left(F\right).$

The solution is investigated using fixed point theorem and Picard-Lindel of $J\left(t\right)=W\left(J\left(t\right)\right)$, When the Picard operator, represented as S, is defined as;

$$W:L_{C}^{0}\left(F,R_{+}^{*}\right)\rightarrow L_{C}^{0}\left(F,R_{+}^{6}\right).$$

Therefore, $S\left(J\left(t\right)\right)=J\left(0\right)+\frac{1}{\Gamma\left(\beta\right)}\int_{0}^{t}\left(t-\lambda\right)^{\beta-1}J\left(\lambda,J\left(\lambda\right)\right)d\lambda$

$$\left\|S\left(J_{1}\left(t\right)\right)-S\left(J_{2}\left(t\right)\right)\right\|$$

$$\left\|\frac{1}{\Gamma\left(\beta\right)}\int_{0}^{t}\left(t-\lambda\right)^{\beta-1}\left[B\left(\lambda,B_{1}\left(\lambda\right)\right)-B\left(\lambda,J_{2}\left(\lambda\right)\right)d\lambda\right]\right\|$$

$$\leq \frac{1}{\Gamma(\beta)}\int_0^t (t-\lambda)^{\beta-1}\left\|B(\lambda, J_1(\lambda)) - B(\lambda, J_2(\lambda))d\lambda\right\|$$

$$\leq \frac{\Im}{\Gamma(\beta)}\int_0^t (t-\lambda)^{\beta-1}\|J_1 - J_2\|d\lambda$$

$$\therefore \left\|S(J_1(t)) - S(J_2(t))\right\| \leq \frac{\Im}{\Gamma(\beta+1)S}$$

When $\frac{\Im}{\Gamma(\beta+1)}S \leq 1$ the solution to equations (6) and (7) is unique since the Picard operator produces a contradiction.

3.4. The basic reproduction number (R_0) and model equilibrium point:

"The basic reproduction number, often referred to as the fundamental transmission rate of an infected individual, represents the average number of secondary infections generated by a single person infected with COVID-19 in a fully susceptible population over the course of their infectious period. This metric is derived using the next generation operator method applied to the system of equations governing the disease dynamics [20].

$R_0 = \rho(FV^{-1})$ where ρ is the dominant eigenvalue of FV^{-1}

$$F = \begin{bmatrix} 0 & \phi & \phi & \phi \\ 0 & 0 & 0 & 0 \\ 0 & 0 & 0 & 0 \\ 0 & 0 & 0 & 0 \end{bmatrix}, V = \begin{bmatrix} K_1 & 0 & 0 & 0 \\ -\varepsilon_1 & K_2 & 0 & 0 \\ 0 & -\alpha_1 & \alpha_2 & -\alpha_1 \\ 0 & -\omega & 0 & K_3 \end{bmatrix},$$

$$FV^{-1} = \begin{bmatrix} \frac{\phi\varepsilon_1}{K_1K_2} + \frac{\phi\alpha_1\varepsilon_1(\omega+K_3)}{K_1K_2\alpha_2K_3} + \frac{\phi\omega\varepsilon_1}{K_1K_2K_3} & \frac{\phi}{K_2} + \frac{\phi\alpha_1(\omega+K_3)}{K_2\alpha_2K_3} + \frac{\phi\omega}{K_1K_2} & \frac{\phi}{\alpha_2} & \frac{\phi\alpha_1}{\alpha_2K_3} + \frac{\phi}{K_3} \\ 0 & 0 & 0 & 0 \\ 0 & 0 & 0 & 0 \\ 0 & 0 & 0 & 0 \end{bmatrix}$$

$$R_0 = \frac{\phi\varepsilon_1(\omega\alpha_1 + \omega\alpha_2 + K_3\alpha_1 + K_3\alpha_2)}{K_1K_2\alpha_2K_3} \quad \text{Where } K_1 = (\varepsilon_1 + \mu)\ K_2 = (\alpha_1 + \omega + \mu)\ K_3 = (\alpha_1 + \mu)$$

3.5 Endemic equilibrium point

An endemic equilibrium point refers to a steady-state condition in which the disease continues to exist within the population at a constant level over time. At this point, the number of infected individuals remains stable rather than declining to zero, indicating the sustained presence of the disease [24]. This positive and stable state, where the infection does not die out but persists within the community, is termed the endemic equilibrium.

At the endemic equilibrium point,

$$\frac{dS}{dt}=\frac{dE}{dt}=\frac{dI}{dt}=\frac{dT}{dt}=\frac{dD}{dt}=\frac{dR}{dt}=0.$$

Let $\varepsilon^{**}=\left(S^{**},E^{**},I^{**},T^{**},D^{**},R^{**}\right)$ be the endemic equilibrium point.

Therefore,

$$S^{**}=\frac{\Lambda}{(\lambda^{**}+\mu)}$$

$$E^{**}=\frac{\lambda^{**}\Lambda}{(\lambda^{**}+\mu)(\varepsilon_1+\mu)}$$

$$I^{**}=\frac{\lambda^{**}\Lambda\varepsilon_1}{(\lambda^{**}+\mu)(\varepsilon_1+\mu)(\alpha_1+\omega+\mu)}$$

$$T^{**}=\frac{\lambda^{**}\Lambda\varepsilon_1\omega}{(\lambda^{**}+\mu)(\varepsilon_1+\mu)(\alpha_1+\omega+\mu)(\alpha_1+\mu)}$$

$$D^{**}=\frac{\lambda^{**}\Lambda\alpha_1\varepsilon_1\omega+\lambda^{**}\Lambda\alpha_1\varepsilon_1}{\alpha_2(\lambda^{**}+\mu)(\varepsilon_1+\mu)(\alpha_1+\omega+\mu)(\alpha_1+\mu)}$$

$$R^{**}=\frac{\lambda^{**}\Lambda\gamma\varepsilon_1\omega}{\mu(\lambda^{**}+\mu)(\varepsilon_1+\mu)(\alpha_1+\omega+\mu)(\alpha_1+\mu)}$$

Substituting into the force of infection of the COVID-19 model, yields the endemic polynomial as

$$\lambda\left(a_0\lambda^2+a_1\lambda+a_2\right)=0,$$

$$\left(a_0\lambda^2+a_1\lambda+a_2\right)=0$$

Where,

$$a_0=\left(\alpha_1+\mu\right)\left(\varepsilon_1+\mu\right)\alpha_2\left(\alpha_1+\omega+\mu\right)$$

$$\times\Lambda\left(\mu^3\alpha_2+\alpha_2\left(\omega+2\alpha_1+\varepsilon_1\right)\mu^2+\left(\left(\alpha_1+\varepsilon_1\right)\alpha_2+\varepsilon_1\right)\left(\alpha_1+\omega\right)\mu+\gamma\omega\alpha_2\varepsilon_1\right)>0$$

$$a_1=2\mu\left(\begin{array}{l}\left(\begin{array}{l}\mu^3+\left(\omega+2\alpha_1+\varepsilon_1\right)\mu^2+\left(\left(-\phi/2+\omega+3/2\alpha_1\right)\varepsilon_1+\alpha_1\left(\alpha_1+\omega\right)\right)\mu\\ -1/2\left(-\alpha_1{}^2+(\phi-\omega)\alpha_1+\omega(\phi-\gamma)\right)\varepsilon_1\end{array}\right)\alpha_2\\ +1/2\varepsilon_1\left(\alpha_1+\omega\right)(\mu-\phi)\end{array}\right)$$

$$\times\alpha_2\left(\varepsilon_1+\mu\right)\left(\alpha_1+\omega+\mu\right)\left(\alpha_1+\mu\right)\Lambda$$

$$a_2=\Lambda\left(\alpha_1+\mu\right)\mu^2\left(\varepsilon_1+\mu\right)\left(\left(\alpha_1+\omega+\mu\right)\left(\mu^2+\left(\alpha_1+\varepsilon_1\right)\mu-\varepsilon_1\left(\phi-\alpha_1\right)\right)\alpha_2-\phi\varepsilon_1\left(\alpha_1+\omega\right)\right)$$

$$\times\alpha_2\left(\alpha_1+\omega+\mu\right)\left(1-R_0\right)>0$$

Whenever $R_0<1$

At the endemic equilibrium, $\lambda\neq0$, thus,

The endemic equilibria of the model (1) can be obtained by solving for λ in the polynomial of the endemic polynomial and substituting the positive values of λ into the endemic

equilibrium points. The quadratic equation can be analyzed for the possibility of multiple equilibria when $R_0 < 1$. Hence, the following result is obtained.

Theorem 2

The model (1) has

(i) a unique endemic equilibrium if $a_2 < 0 \Rightarrow R_0 > 1$.

(ii) a unique endemic equilibrium if $(a_1 < 0$ and $a_2 = 0)$ or $a_1^2 - 4a_0a_2 = 0$

(iii) two endemic equilibria if $a_2 > 0, a_1 < 0$ and $a_1^2 - 4a_0a_2 > 0$

(iv) no endemic equilibrium otherwise.

Therefore, case (ii) of Theorem 2 indicates the potential occurrence of a backward bifurcation, a scenario in which a locally asymptotically stable (LAS) disease-free equilibrium coexists with a LAS endemic equilibrium, even when the basic reproduction number is below one [25, 27]. From an epidemiological perspective, this phenomenon implies that the traditional condition of having the basic reproduction number less than one, while still necessary, is no longer sufficient to guarantee the elimination of the disease from the population.

3.6 Sensitivity Analysis of the covid-19 Model

"Sensitivity analysis plays a vital role in mathematical modeling by evaluating how changes in model parameters affect the resulting outcomes. This process provides valuable insights into the reliability and stability of the model's predictions. In the realm of infectious disease modeling, sensitivity analysis is particularly useful for pinpointing the parameters that most significantly influence disease transmission dynamics, including factors like infection prevalence, the peak of an outbreak, and the effectiveness of control measures [27, 28]. A widely used method involves adjusting one parameter at a time while keeping the others constant, then observing the corresponding changes in model results. Sensitivity is often quantified using measures such as sensitivity coefficients, which represent the partial derivatives of outputs with respect to the parameters. Parameters associated with larger sensitivity coefficients are considered more impactful in determining disease dynamics and are thus prioritized in both intervention planning and model refinement [26].

The sensitivity index of the reproduction number of the model with respect to any parameter say x is given by:

$$\Im_x^{R_0} = \frac{\partial R_0}{\partial x} \times \frac{x}{R_0}$$

Given that

$$R_0 = \frac{\phi\varepsilon_1\left(\omega\alpha_1 + \omega\alpha_2 + K_3\alpha_1 + K_3\alpha_2\right)}{K_1K_2\alpha_2K_3}$$

$$\Im_{\phi}^{R_0} = 1.0000$$

$$\Im_{\omega}^{R_0} = -\frac{\mu\omega}{(\alpha_1+\omega)(\alpha_1+\omega+\mu)} = -0.2507$$

$$\Im_{\alpha_1}^{R_0} = -\frac{\alpha_1(\alpha_1^2\alpha_2 + ((2\mu-2\alpha_2)\omega - 2\alpha_2\mu)\alpha_1 + (\mu-\alpha_2)\omega^2 + \mu(\mu-\alpha_2)\omega - \mu^2\alpha_2)}{(\alpha_1+\omega)(\alpha_1+\mu)(\alpha_1+\alpha_2)(\alpha_1+\omega+\mu)} = 0.2848$$

$$\Im_{\varepsilon_1}^{R_0} = -\frac{\mu}{\varepsilon_1+\mu} = 0.7334$$

$$\Im_{\mu}^{R_0} = -\frac{(\alpha_1^2 + (2\mu+\omega)\alpha_1 + \mu^2 + 2\omega\mu + \omega\varepsilon_1)\mu}{(\varepsilon_1+\mu)(\alpha_1+\mu)(\alpha_1+\omega+\mu)} = -0.7805$$

$$\Im_{\alpha_2}^{R_0} = -\frac{\alpha_1}{\alpha_1+\alpha_2} = 0.9869$$

e

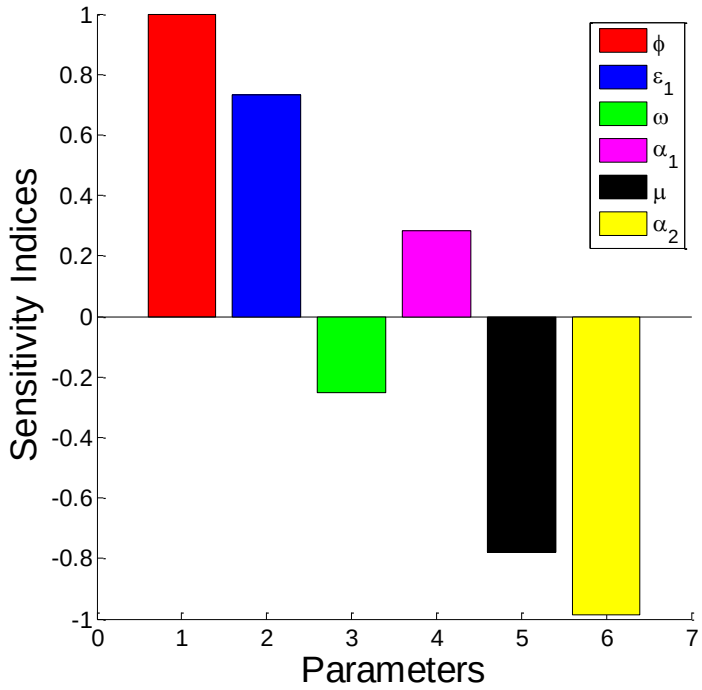

Figure 2. Sensitivity bar chart

The results of the sensitivity analysis reveal that parameters with positive sensitivity indices—such as the rate at which exposed individuals progress to becoming infected—contribute to the increased spread of COVID-19 within the population. Therefore, strategies aimed at reducing this progression rate could help curb transmission [24, 25]. On the other hand, parameters with negative sensitivity indices such as the treatment rate are associated with a decrease in disease prevalence. This implies that enhancing treatment efforts can play a significant role in controlling the spread of the virus among the population.

4.1. Implementation of fractional Adams–Bashforth–Moulton method

This study employs the approach developed by [21-22]. To find an approximate solution to the fractional tuberculosis model given in equation (6), we applied the fractional Adams–Bashforth–Moulton method.

The fractional model (6) is presented as follows:

$$
\begin{aligned}
&{}^{a}D_{t}^{\beta}Z(t)=Y\left(t,Z(t)\right),\ 0<t<\Im,\\
&Z^{(n)}(0)=Z_{0}^{(n)},\ n=1,0,\ldots,Z,Z=[\beta].
\end{aligned}
\tag{24}
$$

Where $Z=\left(S^{*},E^{*},I^{*},T^{*},D^{*},R^{*}\right)\in R_{+}^{6}$ and $Q\left(t,Y(t)\right)$ is a real valued function that is continuous.

Therefore, the following representation of equation (24) can be made using the idea of a fractional integral:

$$
Z(t)=\sum_{n=0}^{Z-1}Z_{0}^{(n)}\frac{t^{n}}{n!}+\frac{1}{\Gamma(\beta)}\int_{0}^{t}(t-x)^{\beta-1}Q\left(x,Z(x)\right)dx \tag{25}
$$

From the method described by [6] and letting the step size $g=\frac{\Im}{N}$, $N\in \mathrm{N}$ with a grid that is uniform on $[0,\Im]$. Where $t_{c}=cr$, $c=0,1,1,\ldots N$. Therefore, the fractional order model of COVID-19 model presented in (6) can be approximated as :

$$
\begin{aligned}
S_{k+1}(t)&=S_{0}+\frac{g^{\beta}}{\Gamma(\beta+2)}\left\{\Lambda-\left(\phi(I^{n}+D^{n}+T^{n})\right)\frac{S^{n}}{N}+\mu S^{*}\right\}+\\
&\frac{g^{\beta}}{\Gamma(\alpha+2)}\sum_{x=0}^{k}dx,k+1\left\{\Lambda-\left(\phi(I_{x}+D_{x}+T_{x})\right)\frac{S_{x}}{N}+\mu S_{x}\right\},\\
E_{k+1}(t)&=E_{0}+\frac{g^{\beta}}{\Gamma(\beta+2)}\left\{\left(\phi(I^{n}+D^{n}+T^{n})\right)\frac{S^{n}}{N}-K_{1}E^{n}\right\}+\\
&\frac{g^{\beta}}{\Gamma(\alpha+2)}\sum_{x=0}^{k}dx,k+1\left\{\left(\phi(I_{x}+D_{x}+T_{x})\right)\frac{S_{x}}{N}-K_{1}E_{x}\right\},\\
I_{k+1}(t)&=I_{0}+\frac{g^{\beta}}{\Gamma(\beta+2)}\left\{\varepsilon_{1}E^{n}-K_{2}I^{n}\right\}+\\
&\frac{g^{\beta}}{\Gamma(\alpha+2)}\sum_{x=0}^{k}dx,k+1\left\{\varepsilon_{1}E_{x}-K_{2}I_{x}\right\},\\
T_{k+1}(t)&=T_{0}+\frac{g^{\beta}}{\Gamma(\beta+2)}\left\{\omega I^{n}-K_{3}T^{n}\right\}+\\
&\frac{g^{\beta}}{\Gamma(\alpha+2)}\sum_{x=0}^{k}dx,k+1\left\{\omega I_{x}-K_{3}T_{x}\right\},
\end{aligned}
$$

$$D_{k+1}(t) = D_0 + \frac{g^{\beta}}{\Gamma(\beta+2)}\left\{\alpha_1 I^n + \alpha_1 T^n - \alpha_2 D^n\right\} +$$

$$\frac{g^{\beta}}{\Gamma(\alpha+2)}\sum_{x=0}^{k} dx, k+1\left\{\alpha_1 I_x + \alpha_1 T_x - \alpha_2 D_x\right\},$$

$$R_{k+1}(t) = R_0 + \frac{g^{\beta}}{\Gamma(\beta+2)}\left\{\gamma T^n - \mu R^n\right\} +$$

$$\frac{g^{\beta}}{\Gamma(\alpha+2)}\sum_{x=0}^{k} dx, k+1\left\{\gamma T_x - \mu R_x\right\},$$

Where

$$S_{k+1}(t) = \frac{1}{\Gamma(\beta)}\sum_{x=0}^{k} e_x k+1\left\{\Lambda - \left(\phi(I_x + D_x + T_x)\right)\frac{S_x}{N} + \mu S_x\right\},$$

$$E_{k+1}(t) = \frac{1}{\Gamma(\beta)}\sum_{x=0}^{k} e_x k+1\left\{\left(\phi(I_x + D_x + T_x)\right)\frac{S_x}{N} - K_1 E_x\right\},$$

$$I_{k+1}(t) = \frac{1}{\Gamma(\beta)}\sum_{x=0}^{k} e_x k+1\left\{\varepsilon_1 E_x - K_2 I_x\right\},$$

$$T_{k+1}(t) = \frac{1}{\Gamma(\beta)}\sum_{x=0}^{k} e_x k+1\left\{\omega I_x - K_3 T_x\right\},$$

$$D_{k+1}(t) = \frac{1}{\Gamma(\beta)}\sum_{x=0}^{k} e_x k+1\left\{\alpha_1 I_x + \alpha_1 T_x - \alpha_2 D_x\right\},$$

$$R_{k+1}(t) = \frac{1}{\Gamma(\beta)}\sum_{x=0}^{k} e_x k+1\left\{\gamma T_x - \mu R_x\right\}, (27)$$

Equations (25) and (26) yield;

$$dx,_{K+1} = K^{\beta+1} - (k-\beta)(k+\beta)^{\beta},\ x = 0$$

$$(k-x+2)^{\beta+1} + (k-\beta)^{\beta+1} - 2(k-x+1)^{\beta+1},\ 1 \le x \le k$$

$$1, x = k+1$$

And

$$e_{x,k+1} = \frac{g^{\beta}}{\beta}\left[(k-x+1)^{\beta}(k-x)^{\beta}\right],\ 0 \le x \le k.$$

Table 2. Parameter used for simulations

Parameter	Value	Source
Λ	$\frac{10000}{59\times 365}$	Estimated
μ	0.5000	[28]
ϕ	0.6000	[28]
γ	0.106	Assumed
α_1	0.150	[28]

ε_1	0.5000	[28]
α_2	0.2000	[28]
ω	0.9700	[28]

4. 2 Fractional order COVID-19 model simulation

The results obtained from numerical simulation of the fractional order COVID-19.

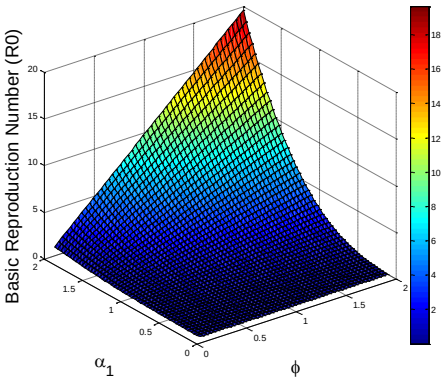

(a) Impact of α_1 and ϕ on R_0

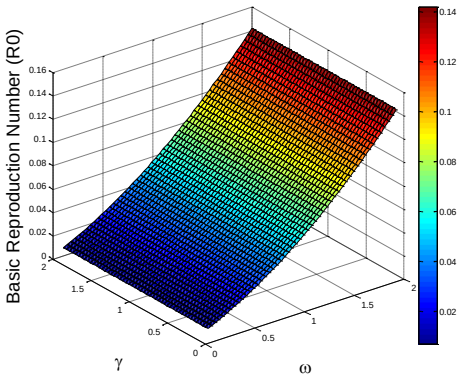

(b) Impact of γ and ω on R_0

Fig 3: surface plot of the basic reproduction number

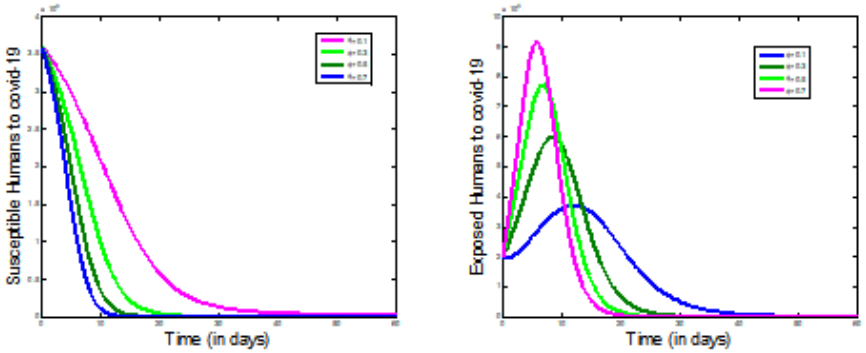

(a) Simulation of Susceptible Humans to Covid-19

(b) Simulation of Exposed Humans to Covid-19

Fig 4: Effect of ϕon $S(t)$and $E(t)$

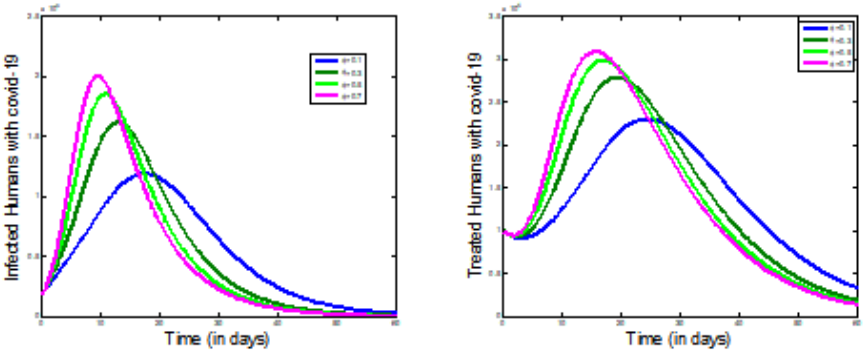

(a) Simulation of infected Humans with Covid-19

(b) Simulation of treated Humans with Covid-19

Fig 5: Effect of ϕon $I(t)$and $T(t)$

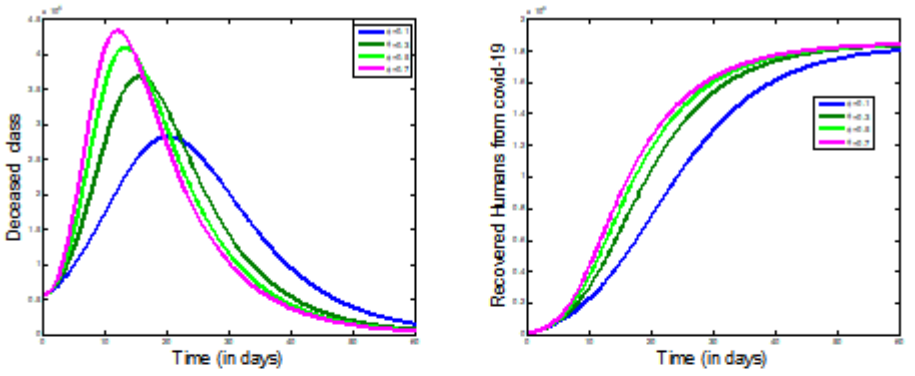

(a) Simulation of Covid-19 Deceased Humans

(b) Simulation of Recovered Humans from Covid-19

Fig 6: Effect of ϕ on $D(t)$ and $R(t)$

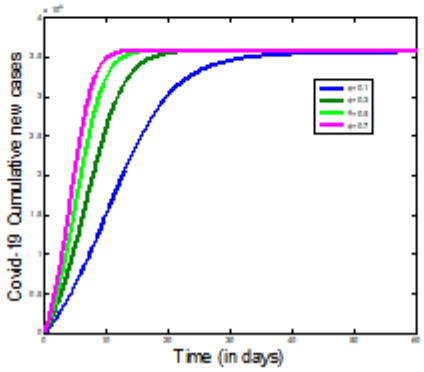

Fig 7: Simulation of Covid-19 cumulative new cases

Figure 3a examines the effect of the contact rate ϕ and the disease-induced death rate α_1 on R_0. The surface shows that R_0 increases as the contact rate ϕ increases, confirming that higher contact rates facilitate more transmission. Conversely, as α_1 increases, R_0 decreases suggesting that a higher death rate reduces the number of secondary infections by shortening the infectious period. However, even at high α_1 values, a high ϕ maintains a relatively high R_0, indicating that high contact can sustain transmission even when mortality is elevated. The surface tilts upward as ϕ increases, reinforcing the importance of reducing contact to control the epidemic.

Figure 3b shows the relationship between the recovery rate γ and treatment rate on R_0. From the plot, it is evident that R_0 decreases as either γ or ω increases. The highest values of R_0 occur when both γ and ω are low, and the lowest values are observed when both parameters are high. This implies that increasing the recovery rate and treatment rate effectively lowers the reproduction number, thereby reducing the potential spread of the disease. The surface curves downward toward higher values of γ and ω, indicating that improving treatment and enhancing recovery synergistically contributes to disease control.

In Figure 4a, the susceptible population is shown to decrease over time, with the rate of decline determined by the value of ϕ. Higher values of ϕ cause a much steeper drop in

susceptible individuals, as more people are exposed to the virus and leave the susceptible class, For lower values of ϕ, the susceptible population declines slowly, suggesting that fewer individuals are becoming infected. This figure highlights the protective effect of lowering contact rates, which prolongs the susceptible state and reduces overall exposure, effectively flattening the epidemic curve. Figure 4b illustrates the trajectory of the exposed population over time for different values of the contact rate ϕ. The exposed compartment consists of individuals who have had contact with the virus but are not yet infectious. As ϕ increases, the curves rise more steeply and peak earlier, reaching significantly higher values. This indicates that a higher contact rate leads to a rapid increase in the number of people exposed to the virus. Following the peak, the curves decline as individuals transition into the infected class. The graph underscores how exposure is extremely sensitive to human interaction levels, with small increases in ϕ leading to markedly higher early outbreak sizes. Figure 5a illustrates the time evolution of the infected population under varying contact rates ϕ. The curves demonstrate that as ϕ increases, the infection spreads more rapidly, resulting in a steeper and earlier peak. The height of the peak is significantly larger for higher ϕ, indicating a much more intense outbreak. Conversely, lower contact rates lead to a slower, more controlled rise in infections, with a later and lower peak. This behavior highlights how crucial it is to manage contact levels, especially early in the epidemic, to prevent overwhelming surges in the infected population.

In figure 5b, the treated classis modeled individuals who are receiving medical care after infection. As ϕ increases, more people become infected and subsequently require treatment. This is reflected in the curves: higher values of ϕ result in a faster rise, an earlier peak, and a higher number of individuals undergoing treatment simultaneously. The pattern indicates a direct relationship between contact intensity and healthcare system burden. For lower ϕ values, the curve is more gradual and the peak is smaller, suggesting a more manageable demand on treatment facilities. This graph is vital for assessing healthcare preparedness and predicting resource needs under different epidemic scenarios. In Figure 6a, the deceased population is modeled as a cumulative outcome over time. The simulation clearly shows that higher contact rates lead to significantly more deaths. With increasing ϕ, the curves climb steeply and reach higher final values, emphasizing the mortality implications of uncontrolled human interaction during an epidemic. The death curves eventually level off, indicating that the outbreak subsides, but the total loss of life is far greater for high ϕ scenarios. This figure serves as a sobering reminder of the human cost of delayed or insufficient intervention strategies.

Figure 6b, presents the growth of the recovered population over time. Recovery is a function of prior infection, so the total number of recoveries is higher when ϕ is high due to the larger number of infections. The curves rise steeply for larger ϕ values and eventually plateau, signifying the epidemic's end as individuals recover and exit the disease cycle. Conversely, smaller ϕ values result in fewer recoveries, not due to delayed healing, but because fewer individuals became infected in the first place. This cumulative behavior illustrates the long-term impact of contact on overall disease burden. Figure 7 presents the cumulative number of

new COVID-19 cases over time. As expected, this curve is always increasing, reflecting the total number of individuals who have contracted the virus. The steepness of the curve is strongly affected by ϕ: higher values produce faster case accumulation and higher final totals. Lower ϕ values yield flatter curves and lower overall case counts. This figure effectively summarizes the epidemic's overall scale and serves as a central indicator of outbreak control effectiveness. It reinforces the conclusion that reducing contact rates can drastically limit the spread of infection across a population.

Conclusion:

This study investigates a fractional-order model that more accurately reflects the real-world dynamics of COVID-19 transmission by incorporating the effects of treatment and the memory-like nature of disease spread. Using Caputo derivatives and the Adams–Bashforth–Moulton method, the model offers a powerful and efficient tool for understanding how the virus evolves over time, especially in response to interventions. The analysis confirms that increasing treatment efforts and reducing contact rates can significantly lower infection levels. Compared to traditional models, this approach provides greater flexibility and realism, making it a valuable asset for guiding public health decisions. Beyond COVID-19, the model has potential applications for other infectious diseases where past states influence future outcomes.

References

1. World Health Organization. (2020, March 11). *WHO director-general's opening remarks at the media briefing on COVID-19*. Retrieved from https://www.who.int/director-general/speeches/detail/who-director-general-s-opening-remarks-at-the-media-briefing-on-covid-19---11-march-2020 (news-medical.net, who.int)
2. Centers for Disease Control and Prevention. (2023). *Science brief: SARS-CoV-2 transmission*. Retrieved from https://www.cdc.gov/coronavirus/2019-ncov/science/science-briefs/transmission.html
3. Guan, W.-J., Ni, Z.-Y., Hu, Y., Liang, W.-H., Ou, C.-Q., He, J.-X., … Zhong, N.-S. (2020). Clinical characteristics of coronavirus disease 2019 in China. *New England Journal of Medicine, 382*(18), 1708–1720. https://doi.org/10.1056/NEJMoa2002032
4. Haug, N., Geyrhofer, L., Londei, A., Dervic, E., Desvars-Larrive, A., Loreto, V., … Klimek, P. (2020, December). Ranking the effectiveness of worldwide COVID-19 government interventions. *Nature Human Behaviour, 4*(12), 1303–1312. https://doi.org/10.1038/s41562-020-01009-0 (nature.com)
5. Mathieu, E., Ritchie, H., Ortiz-Ospina, E., Roser, M., Hasell, J., Appel, C., … Rodes-Guirao, L. (2021). A global database of COVID-19 vaccinations. *Nature Human Behaviour, 5*(7), 947–953. https://doi.org/10.1038/s41562-021-01122-8
6. Riaz, M. B., Aslam, M., Khan, M. A., & Sharif, M. (2024). A nonlinear COVID-19 transmission model with public awareness and environmental factors. *Scientific Reports, 14*(1), 3301. https://doi.org/10.1038/s41598-024-XXXX
7. Aslam, M., & Khan, M. A. (2023). Mathematical modeling of COVID-19 transmission using fractional derivatives. *Mathematics, 11*(2), 456. https://doi.org/10.3390/math11020456
8. Reuters. (2024, October). Japan's Shionogi says COVID pill shows reduced transmission in late-stage trial. *Reuters*. Retrieved from

https://www.reuters.com/business/healthcare-pharmaceuticals/japan-shionogi-covid-pill-shows-reduced-transmission-2024-10-*

9. Time. (2025, March). New antiviral pill helps prevent COVID-19 spread in high-risk households. *Time*. Retrieved from https://time.com/???-new-antiviral-pill-covid-prevention

10. Podlubny, I. (1999). *Fractional differential equations: An introduction to fractional derivatives, fractional differential equations, to methods of their solution and some of their applications* (Vol. 198). Academic Press. Retrieved from https://www.scirp.org/reference/referencespapers?referenceid=1689024 (scirp.org)
11. Tarasov, V. E. (2011). *Fractional dynamics: Applications of fractional calculus to dynamics of particles, fields and media*. Springer. https://doi.org/10.1007/978-3-642-14003-7 (link.springer.com)
12. Diethelm, K., Ford, N. J., & Freed, A. D. (2002). A predictor–corrector approach for the numerical solution of fractional differential equations. *Nonlinear Dynamics, 29*(1–4), 3–22. https://doi.org/10.1023/A:1016592219341 (link.springer.com)
13. Baskonus, H. M., & Agarwal, P. (2020). Numerical solutions to fractional-order epidemic mathematical models using the Adams–Bashforth–Moulton method. *Chaos, Solitons & Fractals, 131*, 109443. https://doi.org/10.1016/j.chaos.2019.109443 (sciencedirect.com)
14. Li, X., Wang, Y., & Chen, J. (2022). Fractional-order SEIR model with quarantine and vaccination for COVID-19 dynamics. *Applied Mathematics and Computation, 420*, 126889. https://doi.org/10.1016/j.amc.2021.126889
15. Zhang, H., & Wei, Y. (2023). Analysis of a fractional SIRS tuberculosis model with treatment and reinfection. *Communications in Nonlinear Science and Numerical Simulation, 120*, 106978. https://doi.org/10.1016/j.cnsns.2023.106978
16. Kumar, R., Singh, A., & Mishra, P. (2021). A fractional SEIQR model for dengue fever incorporating vector dynamics and seasonality. *Mathematical Biosciences, 337*, 108622. https://doi.org/10.1016/j.mbs.2021.108622
17. Chen, L., & Li, M. (2024). Fractional-order SI model for hepatitis B with vaccination and treatment delays. *Journal of Computational and Applied Mathematics, 417*, 114977. https://doi.org/10.1016/j.cam.2023.114977

18. Milici, C., Draganescu, G., & Machado, J. T. (2018). *Introduction to fractional differential equations*. Springer. https://doi.org/10.1007/978-3-319-94557-7
19. Podlubny, I. (1998). *Fractional differential equations: An introduction to fractional derivatives, fractional differential equations, to methods of their solutions and some of their applications*. Elsevier. https://doi.org/10.1016/S0076-5392(07)80004-9
20. VandenDriessche, P., & Watmough, J. (2002). Reproduction numbers and sub-threshold endemic equilibria for compartmental models of disease transmission. *Mathematical Biosciences, 180*(1–2), 29–48. https://doi.org/10.1016/S0025-5564(02)00108-6
https://www.sciencedirect.com/science/article/pii/S0025556402001086
21. Baskonus, H. M., & Bulut, H. (2015). On the numerical solutions of some fractional ordinary differential equations by fractional Adams–Bashforth–Moulton method. *Open Mathematics, 13*, 1–11. https://doi.org/10.1515/math-2015-0001
https://www.degruyter.com/document/doi/10.1515/math-2015-0001/html
22. Agbata, B. C., Agbebaku, D. F., Odo, C. E., Ojih, J. T., Shior, M. M., & Ezugorie, I. G. (2024). A mathematical model for the transmission dynamics of COVID-19 in

Nigeria and its post-effects. *International Journal of Mathematical Analysis and Modelling*, *7*(2), 523–547. https://tnsmb.org/journal/index.php/ijmam/article/view/191

23. Agbata, B. C., Obeng-Denteh, W., Amoah-Mensah, J., Kwabi, P. A., Shior, M. M., Asante-Mensa, F., & Abraham, S. (2024). Numerical solution of fractional order model of measles disease with double dose vaccination. *Dutse Journal of Pure and Applied Sciences (DUJOPAS)*, *10*(3b), 202–217. https://www.ajol.info/index.php/dujopas/article/view/281624
24. Diethelm, K. (1999). The FracPECE subroutine for the numerical solution of differential equations of fractional order. [Unpublished software/documentation]. http://www.fracdiff.org
25. Liu, B., Farid, S., Ullah, S., Altanji, M., Nawaz, R., & Teklu, S. W. (2023). Mathematical assessment of Monkeypox disease with the impact of vaccination using a fractional epidemiological modeling approach. *Scientific Reports*. https://doi.org/10.1038/s41598-023-40745-x https://www.nature.com/articles/s41598-023-40745-x
26. Acheneje, G. O., Omale, D., Agbata, B. C., Atokolo, W., Shior, M. M., & Bolawarinwa, B. (2024). Approximate solution of the fractional order mathematical model on the transmission dynamics of the co-infection of COVID-19 and Monkeypox using the Laplace-Adomian decomposition method. *International Journal of Mathematics and Statistics Studies*, *12*(3), 17–51. https://eajournals.org/ijmss/vol12-issue-3-
27. Agbata, B. C., Omale, D., Ojih, P. B., & Omatola, I. U. (2019). Mathematical analysis of chickenpox transmission dynamics with control measures. *Continental Journal of Applied Sciences*, *14*(2), 6–23. https://www.researchgate.net/publication/344234584
28. Agbata, B. C., Shior, M. M., Obeng-Denteh, W., Omotehinwa, T. O., Paul, R. V., Kwabi, P. A., & Asante-Mensa, F. (2023). A mathematical model of COVID-19 transmission dynamics with effects of awareness and vaccination program. *Journal of Ghana Science Association*, *21*(2), 59–61. https://www.researchgate.net/publication/379485392_